Atomic response to strong laser pulses

D. A. Wasson and S. E. Koonin
W. K. Kellogg Radiation Laboratory, California Institute of Technology, Pasadena, California 91125
(Received 28 August 1987)

We formulate a semiclassical model for the collective response of an atom to a strong laser pulse and use it to study the behavior of the valence shell of xenon. We find that, in a monochromatic wave, a fraction of the shell ionizes rapidly and the rest is driven coherently. The energy distributions of the emitted electrons show reasonable agreement with experimental distributions that are generated via single-particle ionization, indicating that the spectra are independent of the ionization dynamics. The remaining part of the shell is driven coherently and expands with time, thus exerting minimal effect on the core. We also analyze the effects of pulse shape, pulse duration, and the ponderomotive potential. In particular, we present results for femtosecond pulses.

I. INTRODUCTION

The study of the response of atoms to electromagnetic radiation in the nonperturbative regime is now possible experimentally. A variety of effects have been observed or are predicted to occur in this novel situation, including multiple ionization. In weak fields, this multi-ionization occurs sequentially: one electron absorbs many photons and escapes, followed by more electrons doing the same, with the ion being in its ground state at each step. In strong fields, however, a strong collective response is possible, that is, several electrons (possibly a whole shell) respond at once to the applied field.

Several qualitative analysis of collective behavior have been performed,[1] although it has not yet been observed experimentally.[2] In these experiments, the shape of the applied laser pulse plays an important role. For instance, it has been shown that if the rise time of the pulse is slow enough (as it is in the current experiments), then the initial ionization will occur in the perturbative regime.[3] To study the true response of an atom to a strong field, pulses with short rise times will have to be used, making it necessary to understand the effect of the pulse envelope.

Experiments also show that the ionized electrons can absorb many more photons than the minimum required for ionization. The energy spectra that result are completely different from those predicted by perturbation theory.[4] Data show that the structure of the spectra is determined primarily by the intensity and frequency of the applied field and not by the particular atom.[5]

An accurate description of these findings could be obtained from solutions to the time-dependent many-body Schrödinger equation, which are, of course, impossible at present. Several approximate methods have been applied. Perturbation theory has been used to study both the electron energy spectra[6] and the many-electron response,[7] but it lacks the ability to study the strong-field regime with any confidence. Direct numerical integration of the Hartree equations shows promise for understanding the ionization and excitation of the atom, but is as yet unable to describe the emitted electrons or sufficiently large atoms.[8]

We have approached the problem of atoms in intense light using a semiclassical model. This allows us to describe all of the experimental observables simultaneously for arbitrary pulse shapes. In particular, we are able to study the characteristics of collective motion of the shell and the envelope of the energy spectra of the ionized electrons. In Sec. II we describe our model and its numerical implementation, while in Sec. III we present some results.

II. SEMICLASSICAL MODEL OF THE VALENCE SHELL

This section develops our model for analyzing the response of the valence shell of an atom, assuming an inert core. We restrict ourselves to the valence shell since experiments studying multiple ionization indicate that it is mainly the valence shell that interacts with the external field,[9] although our model can be extended easily to several shells or even to the whole atom. In Sec. II A we discuss the motivation behind our calculation and compare it with related methods. To track the evolution of the valence shell, we need both an initial classical approximation to the valence shell and then a means of evolving it in time. We discuss these two issues in Secs. II B and II C, respectively.

A. The model

Our model, which has been previously used with success in time-dependent nuclear physics problems,[10] finds a rigorous basis as a semiclassical expansion of the time-dependent Hartree-Fock (TDHF) equations, with the addition of short-range correlation effects. The semiclassical approximation to TDHF equations describes collective motion in the time varying mean field of the atom. Although we introduce additional correlation effects, our model does not describe single-electron excitations. Hence, our model is good for analyzing the process of collective excitation, but not in deciding when this is the dominant excitation mechanism. We now describe the model.

The many-body wave function of the shell can be approximated in terms of single-particle wave functions ψ_i

by a Slater determinant, $\Psi_{\text{shell}} \propto \det[\psi_i(x_j)]$. From this we can construct the Wigner function, which behaves like a classical phase-space distribution,

$$f(\mathbf{r},\mathbf{p},t) = \int d^3\mathbf{s}\, e^{(i\mathbf{p}\cdot\mathbf{s})/\hbar} \sum_i \psi_i(\mathbf{r}-\mathbf{s}/2,t) \times \psi_i^*(\mathbf{r}+\mathbf{s}/2,t) \ . \quad (1)$$

Integrating over the $\mathbf{r}$ dependence of f leads to the momentum density, while integrating over the $\mathbf{p}$ dependence of f leads to the spatial density. In addition, in the semiclassical regime, the Wigner function evolves in time via the Boltzmann equation,

$$\frac{\partial f}{\partial t} + \frac{\mathbf{p}}{m}\cdot\nabla_{\mathbf{r}} f - \nabla_{\mathbf{r}} v \cdot \nabla_{\mathbf{p}} f = \left.\frac{\partial f}{\partial t}\right|_{\text{coll}} , \quad (2)$$

as does the classical phase-space distribution.

To see how this comes about, consider the TDHF approximation, in which the wave functions obey single-particle equations of the form

$$\left[-\frac{\hbar^2}{2m}\nabla^2 + v[\rho(\mathbf{r},t),\mathbf{r},t]\right]\psi_i = i\hbar\frac{\partial\psi_i}{\partial t} \ , \qquad \rho(r,t) = \sum_i |\psi_i(r,t)|^2 \ . \quad (3)$$

It follows that

$$\frac{\partial f}{\partial t} + \frac{\mathbf{p}}{m}\cdot\nabla_{\mathbf{r}} f - \frac{2}{\hbar}\sin\left[\frac{\hbar}{2}\nabla_{\mathbf{r}}^{v}\cdot\nabla_{\mathbf{p}}^{f}\right] v f = 0 \ , \quad (4)$$

which implies the Vlasov equation in the classical limit ($\hbar \to 0$),

$$\frac{\partial f}{\partial t} + \frac{\mathbf{p}}{m}\cdot\nabla_{\mathbf{r}} f - \nabla_{\mathbf{r}} v \cdot \nabla_{\mathbf{p}} f = 0 + O(\hbar^2) \ . \quad (5)$$

Correlations beyond the TDHF approximation can be incorporated by adding a collision term that respects the Pauli exclusion principle [$f(\mathbf{r},\mathbf{p}) < 1$]. However, there is no unique prescription for determining this collision term. We use the standard Uehling-Uhlenbeck form,

$$\left.\frac{\partial f}{\partial t}\right|_{\text{coll}}(p_1) = \int \frac{d^3p_2 d^3p_3 d^3p_4}{(2\pi)^6}(2\pi)^3\delta^3 \times (p_1+p_2-p_3-p_4)(\sigma_c v_{12}) \times [f_3 f_4(1-f_1)(1-f_2) - f_1 f_2(1-f_3)(1-f_4)] \ , \quad (6)$$

which incorporates the effects of two-body elastic collisions with cross section σ_c into the evolution of the phase-space distribution subject to Pauli blocking.[11] The specific form used for the cross section is described in Sec. II C.

This shows that in the semiclassical limit it is possible to extract a quantum-mechanical quantity that has the properties of (and evolves like) a classical phase-space distribution. In our simulations we generate an initial distribution that approximates that of the shell and then evolve it classically. The specifics of how this is done are discussed in Secs. II B and II C.

An alternate classical approach that we have investigated is to perform molecular dynamics simulations. Kirschbaum and Wilets[12] have introduced classical momentum-dependent electron-electron and electron-nucleus potentials that simulate the Pauli exclusion principle and Heisenberg uncertainty relation and have used them to model atomic muon capture. One could similarly evolve these atoms in an applied electromagnetic field. In this type of simulation one is treating the physical number of electrons as discrete classical particles interacting with each other, while in our calculations we evolve an entire phase-space distribution classically. As there are an infinite number of classical configurations for the ground state of the atom in the Wilets model, performing molecular dynamics simulations for many of these ground states will give results equivalent to those obtained in our method. However, the computational burden is more extensive and the method for dealing with quantum mechanics has no rigorous justification. On the other hand, an advantage of a molecular dynamics simulation is that single-particle and collective excitations can both occur, so that the competition between these two modes of excitation can be studied,[13] something that cannot be studied in our model.

B. The initial distribution

In our calculations we approximate the initial phase-space distribution by a Thomas-Fermi distribution, generated by assuming a uniform electron gas at each point with Fermi momentum

$$k_f(r) = \left[\frac{2m}{\hbar^2}[E_f - v(r)]\right]^{1/2} . \quad (7)$$

Here E_f is the Fermi energy and $v(r)$ is the electrostatic potential obtained by solving Poisson's equation self-consistently,

$$\nabla^2 v(r) = -4\pi e^2\left[\frac{1}{3\pi^2}k_f^3\right] + 4\pi Z e^2\delta(\mathbf{r}) \ , \quad (8)$$

yielding a spherically symmetric charge distribution. E_f is zero for neutral atoms.

We will study the evolution of the valence shell in the presence of a static core. Since there is no shell structure in the Thomas-Fermi atom, we must introduce the distinction between valence shell and core artificially. We separate the core from the valence shell by picking an energy E_{core} such that all electrons with energy below E_{core} are in the core and those with larger energy are in the valence shell. The core is then assumed fixed in time, generating a force $\mathbf{F}_{\text{core}}(\mathbf{r})$ that is directed radially and is spherically symmetric.

The primary advantage of the Thomas-Fermi phase-space distribution is that it is very easy to work with (see Sec. II C). It also gives a good description of the core (except for the smallest radii), which means that the core's influence on the valence electrons is well simulated. One drawback, which we discuss below, is that the initial dis-

tribution of the shell electrons is underbound, as the phase-space distribution extends to zero binding energy. Nonetheless, we believe it provides a good initial model for studying the evolution of an atomic shell in a strong applied field.

C. The evolution

The phase-space distribution discussed above evolves in time via Eq. (2). We accomplish this by discretizing the initial phase-space distribution into N pseudoparticles that move in the mean field v and collide with the cross section σ_c of Eqs. (2) and (6). If the valence shell contains N_{shell} real electrons, then the shell (in the Thomas-Fermi approximation) uniformly occupies a region of phase space of volume $\int d^3p\, d^3x = \frac{1}{2}N_{\text{shell}}h^3$, where the factor of $\frac{1}{2}$ is due to the spin degeneracy of the electrons. This implies that each pseudoparticle occupies a volume in phase space of $N_{\text{shell}}h^3/2N$, which we take to be a cube in coordinate space centered about the position of the pseudoparticle and a cube in momentum space centered about its momentum. This discretizes the initial phase space exactly only in the limit that the number of pseudoparticles is infinite.

We now need to determine the mean field and the collision cross section. To motivate our choice, consider the fully classical calculation in which the pseudoparticles evolve in time via

$$\frac{d\mathbf{p}_i}{dt} = \mathbf{F}_i(\{\mathbf{r}_k\},t) , \qquad \frac{d\mathbf{r}_i}{dt} = \frac{\mathbf{p}_i}{m} , \tag{9}$$

where

$$\mathbf{F}_i(\{\mathbf{r}_k\},t) = -\frac{Ze^2}{|\mathbf{r}_i|^3}\mathbf{r}_i + \mathbf{F}_{\text{core}}(\mathbf{r}_i) + \frac{N_{\text{shell}}}{N}\sum_{\substack{i,j \\ i\neq j}} \frac{e^2}{|\mathbf{r}_i-\mathbf{r}_j|^3}(\mathbf{r}_i-\mathbf{r}_j) - e\mathbf{E}(t) . \tag{10}$$

Here $\mathbf{F}_{\text{core}}(\mathbf{r})$ is the force due to the static core and $\mathbf{E}(t)$ is the external field. We adopt the dipole approximation for $\mathbf{E}$ (i.e., spatial independence) and ignore the magnetic field. The external field is taken to point in the z direction, implying that the system will maintain azimuthal symmetry in time as $N\to\infty$. We construct the mean field and collision cross section so as to mimic Eq. (10) as closely as possible while maintaining the constraint of Pauli blocking. This is accomplished by dividing the electron-electron interaction term of Eq. (10) into a cylindrically symmetric mean field and then generating collisions from the residual interaction.

We determine the mean field by solving Poisson's equation for a smoothed, cylindrically symmetric charge density generated by the positions of the pseudoparticles. To do this, we introduce a lattice and relax the discretized Poisson's equation. We calculate the force from the resulting potential using the difference formula defined by the lattice. This force, together with the force due to the nucleus, core, and external field, defines the net force due to the mean fields $\mathbf{F}_{\text{MF}}(\mathbf{r},t)$.

The motion in the mean field is integrated by leapfrogging the position and momentum with a time step Δt,

$$\mathbf{p}_i[(n+\tfrac{1}{2})\Delta t] = \mathbf{p}_i[(n-\tfrac{1}{2})\Delta t] + \Delta t\,\mathbf{F}_{\text{MF}}(\mathbf{r}_i,t) , \qquad \mathbf{r}_i[(n+1)\Delta t] = \mathbf{r}_i[n\Delta t] + \frac{\Delta t}{m}\mathbf{p}_i[(n+\tfrac{1}{2})\Delta t] . \tag{11}$$

As both the mean field and the charge distribution are cylindrically symmetric, only the ρ and z components of the pseudoparticle motion in the mean field need to be integrated explicitly.

When two pseudoparticles become close, their mutual Coulomb repulsion dominates over the mean field. This generates the collisions discussed in Sec. II A. We handle these by specifying that when two pseudoparticles become close (as determined by our initial phase-space discretization), they scatter elastically, at a randomly chosen impact parameter, through a truncated Coulomb potential. We then check whether these phase-space locations are already occupied, either by other pseudoparticles or by the core. If either phase-space volume is occupied, scattering does not occur. This method corresponds to a stochastic evaluation of the collision integral, Eq. (6).

We end this section by giving the values of the various parameters discussed above that we used in our computations. The simulations are typically performed for the valence shell of xenon ($Z=54$), which contains eight electrons. This corresponds to $E_{\text{cut}} = -11.6$ eV in our Thomas-Fermi model. We discretize this shell with $N=1000$ pseudoparticles. This is large enough to give a good discretization of phase space, yet small enough to be computationally tractable. Each pseudoparticle occupies a volume 0.66^3 eV^3 fs^3 of phase space. We partition this volume between real and momentum space so that each pseudoparticle represents approximately equal portions of each. This results in each pseudoparticle occupying a cube of side 0.5 Å in real space and a cube with sides corresponding to a velocity of 2 Å/fs in momentum space. Collisions are performed when pseudoparticles come to within 0.5 Å of each other. Significant collisions typically require an impact parameter of 0.1 Å and a relative velocity of less than 2 Å/fs. This means that the time scale over which a typical significant collision lasts is of order 0.1 fs which corresponds to the time scale over which we should evaluate successive collisions. In our code, we actually check for collisions every 0.05 fs. The lattice size we use for constructing the mean field is 40×80 with a variable lattice spacing, typically 0.2 Å, so as to always sufficiently encompass the entire bound atom. The time scale over which the mean field has to be updated depends on the speed with which it is evolving; typically it is updated every 0.05 fs. To successfully evolve the system in time, we need a time step of 5×10^{-5} fs. It takes approximately 20 min of CPU time on a Cray X/MP-48 to evolve the system for 10 fs. The computational burden is divided roughly equally among integrat-

ing the equations of motion, solving Poisson's equation, and performing the collisions plus Pauli blocking.

III. RESULTS

We first consider the case in which the atom is exposed to a monochromatic wave. We perform our calculations for a xenon atom in which the shell is taken to be the $n=5$ shell with eight electrons. We first expose the shell to monochromatic waves of frequency $\omega=10^{16}$ Hz (period $=0.63$ fs) corresponding to the frequency used in Rhodes's experiments.[2,9] We study the response up to a peak field strength of 10 V/Å, above which the ponderomotive force begins to become important. These results are discussed in Sec. III A. In Sec. III B we examine the response of the lower half of the xenon shell, assuming that the first half of the xenon shell has been previously ionized leaving the bottom half undisturbed. This allows us to examine the effect of separation energy on the ionization dynamics. In Sec. III C, we consider the effects of the ponderomotive potential and of pulse shape and duration.

A. Response of full valence shell

We expose the full shell to monochromatic waves of varying amplitudes

$$\mathbf{E}(t)=E_0\hat{\mathbf{z}}\sin(\omega t) \tag{12}$$

and examine the evolution of the shell with time. We first look at the ionization of the atom. In our model, ionization is determined by examining the individual energies of the pseudoparticles, with positive-energy pseudoparticles being defined as ionized. The individual energies ϵ_i are calculated as

$$\epsilon_i=\frac{p_i^2}{2m}-\frac{Ze^2}{r_i}+V_{\text{core}}(r_i)+V_{\text{MF}}(r_i)\ , \tag{13}$$

where V_{core} and V_{MF} are the potentials due to the core and shell mean field, respectively.

Figure 1 shows the fraction of positive-energy pseudoparticle as a function of time for various values of E_0 during the first 20 fs of evolution. For strong fields, ionization occurs at a uniform rate followed by a rapid leveling off of the fraction of positive-energy pseudoparticles. The leveling occurs at later times and becomes less abrupt as the strength of the field is decreased. By the time the field has decreased to 0.5 V/Å the kink has almost disappeared with the ionization rate becoming nearly uniform. We also observe fluctuations in the fraction of ionized pseudoparticles after the ionization has leveled off. These are associated with the oscillating field, and will be further discussed in Sec. III C.

We now examine several properties of the calculated ionization. Figure 2 shows the fraction of the shell ionized after 20 fs at various field strengths. The error bars reflect the previously mentioned fluctuation. One can think of this graph as giving the average charge state that will be observed if a pulse with a square 20-fs envelope is applied. Figure 1 shows that the fraction ionized is independent of the pulse length for fields greater than ~ 1 V/Å and pulse lengths greater than 5 fs. For smaller

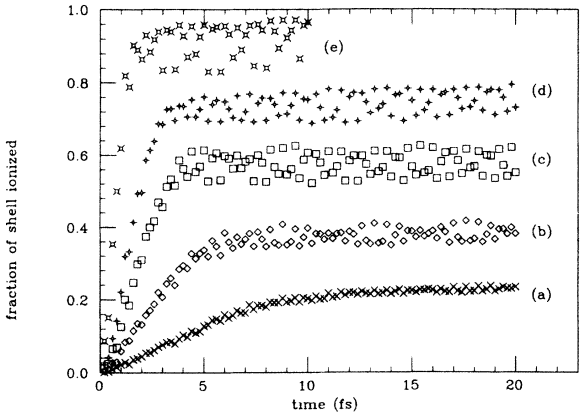

FIG. 1. Fraction of a xenon valence shell ionized as a function of time for peak field strengths of (a) 0.5, (b) 1, (c) 2, (d) 3, and (e) 10 V/Å.

fields, the fraction ionized continues to rise beyond 20 fs. Hence, one prediction of our model is that, in strong fields, the fraction of the shell ionized is independent of the pulse length.

Figure 3 shows the initial ionization rate (slope of Fig. 1 at $t=0$) for various field strengths. This can be interpreted as the rate at which the initial electron is removed. It varies linearly for fields less than ~ 3 V/Å and then gradually levels off. This is to be contrasted with the result from quantum-mechanical perturbation theory in which the ionization rate scales as E_0^{2N}, where N is the number of photons required to ionize the first electron. In our model, the shell extends to zero binding energy so $N=1$. Hence, the scaling of the ionization rate in this collective model is less severe than for single-particle excitation in perturbative quantum mechanics. In Sec. III B, we will see the effect of increasing the binding energy on this scaling.

We now examine the spectra of the emitted electrons, defined as those pseudoparticles with positive energy. In Fig. 4 we show the electron energy spectra for a variety of field strengths after 20 fs of exposure. For large fields, the spectra oscillate with time due to the interaction of the unbound electrons with the field. Thus, we have

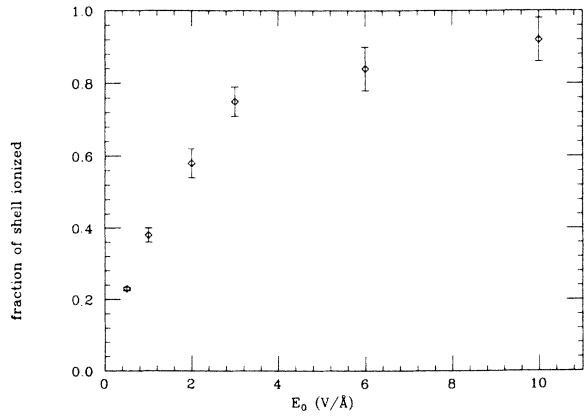

FIG. 2. Fraction of the valence shell ionized after 20 fs as a function of field strength.

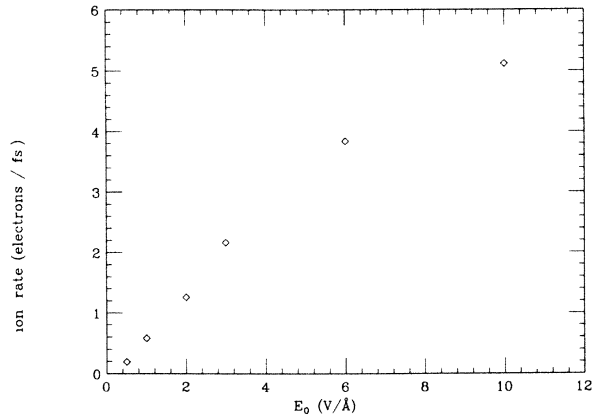

FIG. 3. Initial ionization rate as a function of field strength.

determined the spectra by letting the field strength fall linearly to zero over the final 2 fs ($\sim$3 periods). We observe that the shapes of the spectra are roughly independent of the strength of the field. At the lowest strength, 0.5 V/Å, there is a small uniform high-energy tail that is not seen in the others and at the highest field strength, 10 V/Å, there is a flattening at low energies. Both of these will be commented on later.

The upper panel in Fig. 5 shows the average energy, maximum energy, and energy of the half maximum point of the spectra of the ionized pseudoparticles at various field strengths. This shows that the spectra vary linearly with E_0 except at the lowest field strength plotted. The slope, however, depends on which attribute of the spectra is being observed. For low fields, the maximum energy becomes independent of the field strength. This is because these ionized pseudoparticles are generated by collisions and so their energy is determined by the momenta of the bound pseudoparticles and not the strength of the field. This process occurs because the evolution of the shell opens up phase space, which diminishes the Pauli blocking. When two pseudoparticles collide with momenta characteristic of their binding energy, the collision can ionize one of the particles. This mechanism is more dominant in the Thomas-Fermi atom than in a real atom because the pseudoparticles have kinetic energies greater than their binding energies while in a real atom they have kinetic energies equal to their binding energies. The linear variation of the energy with field for larger fields is because the field changes the kinetic energy of each pseudoparticle at a rate proportional to the field strength,

$$\left[\frac{dT_i}{dt}\right]_{\text{field}} = \frac{e}{m}\mathbf{E}(t)\cdot\mathbf{p}_i \ , \tag{14}$$

where T_i is the kinetic energy of the ith pseudoparticle. Thus, when the energy of the ionized electron is created by the field pushing it from being bound into the continuum, the energy should vary linearly with the field. For higher fields the electron energy spectra is also affected significantly by the field after ionization, as the oscillatory motion of the electron in the free field generates an average energy that becomes equal to and greater than

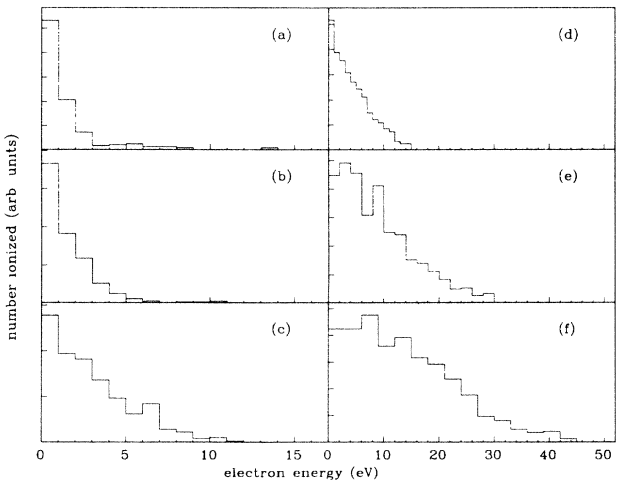

FIG. 4. Energy spectra of ionized pseudoparticles for E_0 = (a) 0.5, (b) 1.0, (c) 2.0, (d) 3.0, (e) 6.0, and (f) 10.0 V/Å.

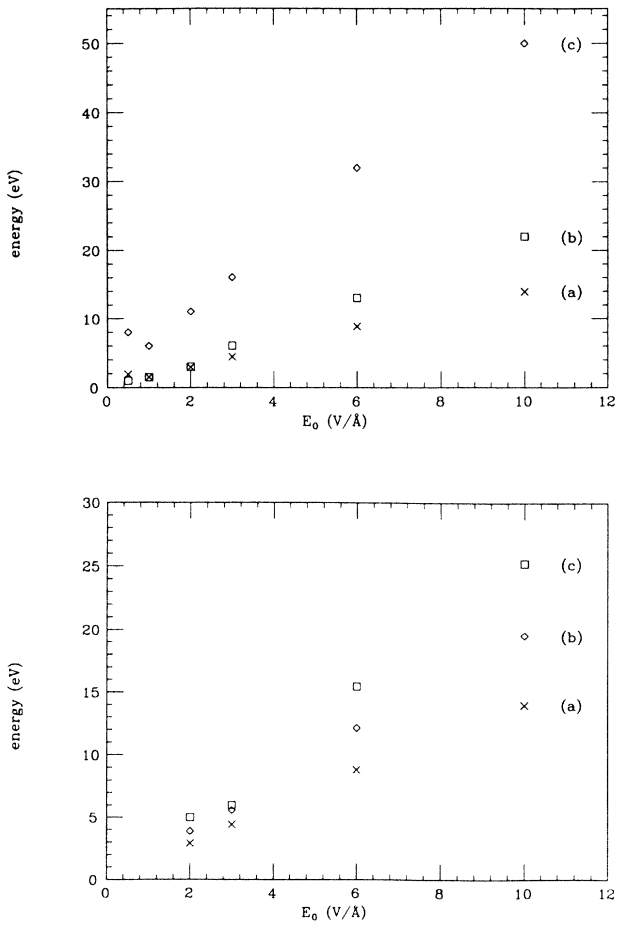

FIG. 5. Upper panel: (a) average energy, (b) energy of half maximum, and (c) maximum energy of the ionized pseudoparticles. Lower panel: Energy of electrons emitted within a core making an angle θ= (a) 90°, (b) 45°, and (c) 30° with the z axis as a function of peak field strength.

the energy absorbed during the ionization. This gives a quadratic variation of the energy with field and will be discussed in Sec. III C. This effect begins to become important in our results near $E_0 = 10$ V/Å, where the average energy of fluctuation is 4 eV.

We note that the energy distributions discussed above are for electrons emitted in all directions. To study the variation of the spectra with emission angle, we restrict our spectra to those ionized pseudoparticles emitted at angles less than 45° and 30° with respect to the z axis; smaller angles cannot be analyzed due to poor statistics. Figure 6 shows the average energy for these two opening angles for different field strengths. The average energy increases with decreasing opening angle, as would be expected from the ionization mechanism discussed previously. Figure 5 shows the scaling of the average energy with the electric field for these two opening angles and the entire spectra. The spectra all scale linearly with the electric field, although the slope becomes steeper with decreasing angle. Finally, Fig. 7 shows the variation of the electron energy spectra with opening angle for a field strength of 2 V/Å, which is representative of the variation of the other energy spectra. We observe that the spectra become more uniform for smaller opening angles, which is consistent with the observation that the faster pseudoparticles tend to have their motion aligned with the z axis.

In Fig. 8 we show experimental electron energy spectra measured by Kruit *et al.*[4] covering all angles of emission. These experiments were performed at a frequency approximately one-fifth of ours using pulses with peak electric fields in the range of 1 V/Å. At this low frequency the ponderomotive force is significant and indeed is believed to be what is responsible for the elimination of the low-energy peaks. In Sec. III C, we will see that the ponderomotive force can be incorporated into our energy spectra by adding the ponderomotive energy to each ionized pseudoparticle. The effect of this is to add an E_0^2 scaling on top of the E_0 scaling already discussed. Since Kruit's data do not extend to the end of the spectra, we cannot compute the average energy of the emitted electrons. Instead, we read off the energy at which the envelope of the spectra has dropped to one-half of its peak value and then subtract the ponderomotive energy. This is plotted in Fig. 8. We observe a linear relation with a slope comparable to the slopes of the curves in Fig. 5.

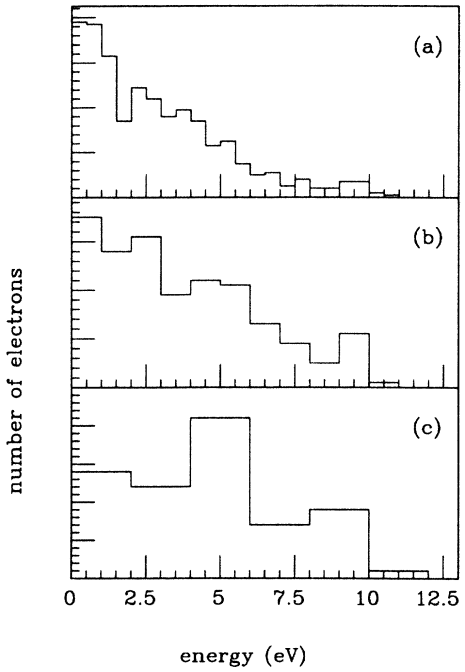

FIG. 7. Energy spectra of the ionized pseudoparticles generated by a 2-V/Å peak field strength for $\theta =$ (a) 90°, (b) 45°, and (c) 30°.

A discrepancy between our results and the experimental data is the scaling of the total ionization rate with applied field strength. The experimental rate scales roughly as the intensity raised to the number of photons required for single-particle ionization and hence cannot be directly compared with our rates since our simulations are at a different frequency. However, as will be seen in Sec. III B, our collective model never generates ionization

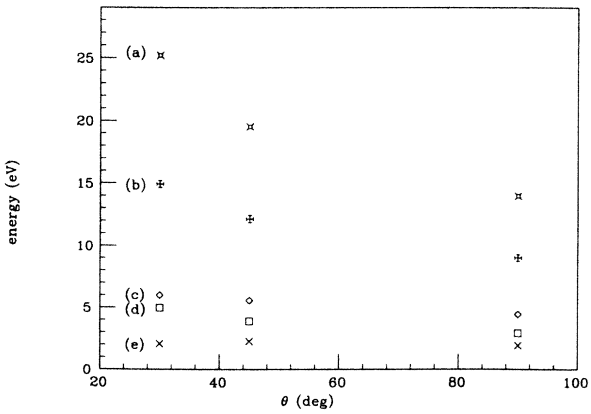

FIG. 6. Average energy of ionized pseudoparticles emitted within an angle θ of the z axis for peak field strengths of (a) 10.0, (b) 6.0, (c) 3.0, (d) 2.0, and (e) 1.0 V/Å.

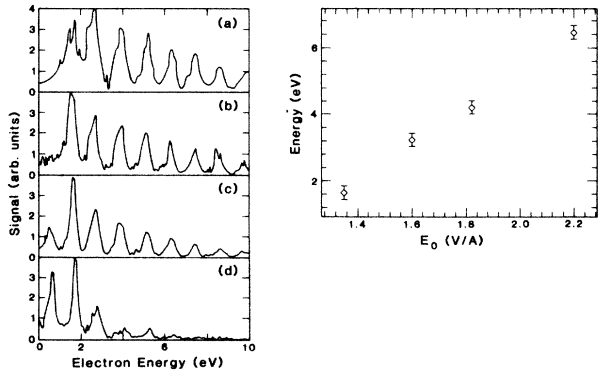

FIG. 8. Experimental electron spectra of Kruit *et al.*[4] (left) and the scaling of the half-full energy of the spectra. The ponderomotive energy has been subtracted from the latter values (right).

rates as extreme as those generated by single-electron response. What is interesting is that although the experiment is dominated by single-electron response and we are calculating the coherent response, the resulting electron energy spectra are similar. This indicates that the shape of the spectra is largely determined at the end of the ionization, as the electron leaves the atom, and is not affected by how the electron was initially excited. It follows that the envelope of the electron energy spectra cannot be used as an indicator of collective ionization.

We now analyze the behavior of those pseudoparticles that remain bound. From Fig. 1 we see that the number of bound pseudoparticles remains essentially constant with time, except for fluctuations. The total energy of the bound particles as a function of time is shown in Fig. 9. The particles are constantly absorbing energy at a rate that diminishes with time. We note that the total energy of the bound particles fluctuates in time due to the fluctuation in the number of bound particles (Fig. 1). There is no evidence that these bound pseudoparticles will ever ionize. In Fig. 10 we plot the rms radius of the bound pseudoparticles against time and observe a uniform expansion. The large fluctuations are due to the fluctuations in the number of ionized particles seen in Fig. 1. The expansion is large even for the strength of 0.5 V/Å where the ionization is the smallest. This happens because as the atom ionizes the Coulomb potential extends far away from the atom. For instance, a net atomic charge of 1 yields a potential 1.4 eV deep at 10 Å. Hence, as the field pumps energy into the shell, it has a large region of space into which it can (and does) expand. Thus, our conclusion is that the bound particles absorb energy and expand in time without ionizing, although the expansion means that at some point in time they will have effectively ionized. A steady coherent oscillation is not set up.

Finally, we examine the effect of collisions on the ionization dynamics. Figure 11 shows the fraction ionized as a function of time for $E_0=0.5$ eV/Å, both with and without collisions. As expected, the collisions increase the fraction of the atom ionized, but the qualitative behavior of the curve is unchanged. All other aspects of the ionization dynamics also behave qualitatively the same with and without collisions. As the field strength is increased, the quantitative effect of the collisions becomes smaller since the more rapid ionization results in fewer collisions.

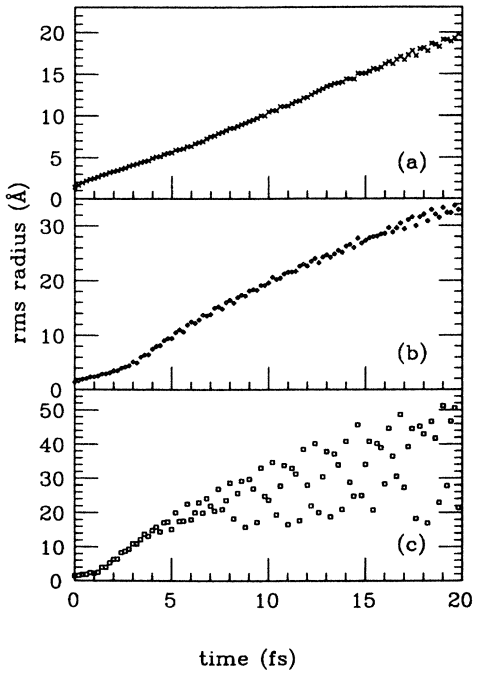

FIG. 10. rms radius of the bound pseudoparticles as a function of time for peak field strengths of (a) 0.5, (b) 2.0, and (c) 6.0 V/Å.

B. Response of a half-full valence shell

It is not clear which of the results above will remain true for a more realistic atomic model, and which are peculiar to the Thomas-Fermi approximation. The most glaring error in the Thomas-Fermi model is the lack of

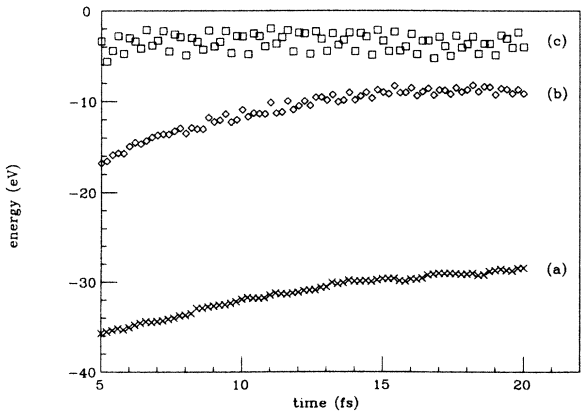

FIG. 9. Total energy of the bound pseudoparticles as a function of time for peak field strengths of (a) 0.5, (b) 2.0, and (c) 6.0 V/Å.

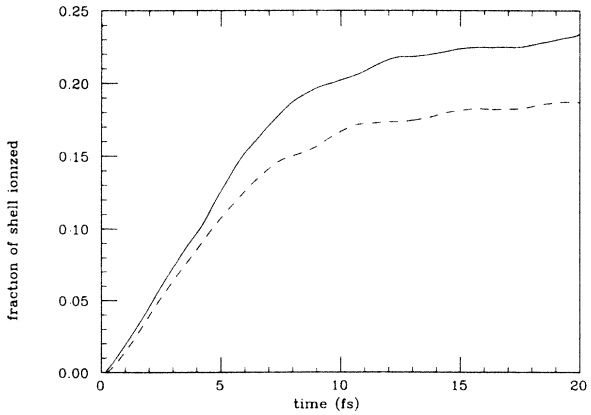

FIG. 11. Effect of collisions on the evolution of the shell. The graph shows fraction ionized as a function of time for $E_0=0.5$ V/Å. The solid line represents the evolution with collisions and the dashed line the evolution without collisions.

separation energy, which clearly has a major effect on the ionization dynamics.

We can investigate the effect of separation energy by removing the top half of the valence shell. This decreases the mean Coulomb field due to the shell, changing the average binding energy per electron from 5 eV to 45 eV. We analyze the response of this half shell and compare it with the response of the full shell.

The ionization as a function of time is shown in Fig. 12. One clearly sees the effect of the separation energy, which requires that a finite amount of energy be put in the system to ionize it. When the field strength is $E_0=3$ V/Å, the atom requires 5 fs to begin ionizing, achieving a uniform ionization rate from 15 to 40 fs and then gradually leveling off at around 60 fs. The 10-V/Å curve rises linearly after about 1 fs and then gradually levels out. Similar behavior is shown by the 6-V/Å curve. The abrupt end of ionization that was seen in the full-shell case is not seen here. We have not integrated far enough in time to see whether or not the entire atom is actually ionized.

In Fig. 13 we show the ionization rates for various field strengths. In this case, the ionization rate is defined as the slope of the linear part of the ionization curve. The scaling of the rate with E_0 is slightly greater than for the full shell, but negligible compared to the scaling that would be expected from quantum-mechanical perturbation theory (the ionization order is 7). We therefore conclude that the scaling of the rates with which the collectively excited shell ionizes is fairly insensitive to the initial binding energy. The magnitude of the ionization rates, however, is very sensitive to the separation energy, the rates being slower for greater separation energy.

Many features of the atomic response are the same for the half and full shells. The half-shell electron energy spectra at a given field strength are quantitatively identical with those of the full shell, despite the different excitation dynamics. This leads us to believe that our electron spectra are independent of the exact atomic model used. The energy and rms radius of the bound pseudoparticles show the same qualitative behavior as those for the full shell.

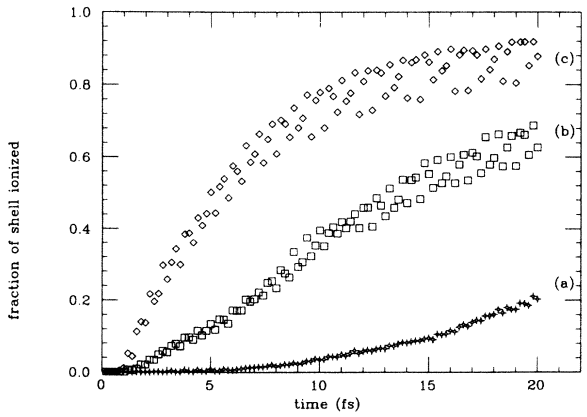

FIG. 12. Fraction of shell ionized as a function of time for an initially half-full outer shell for field strengths of (a) 3, (b) 6, and (c) 10 V/Å.

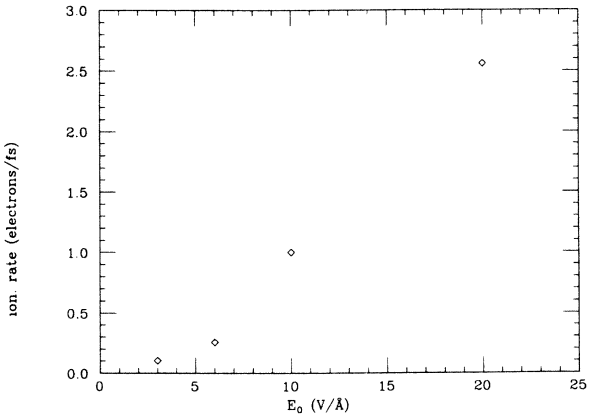

FIG. 13. Initial ionization rate vs E_0 for an initially half-full outer shell.

One prominent difference between the evolution in the half- and full-shell cases is the shape of the oscillating shell. We analyze the shape through the dimensionless quadrupole moment,

$$Q=\frac{\langle 2z^2-\rho^2\rangle}{\langle z^2+\rho^2\rangle}\ . \tag{15}$$

A distribution that is strongly concentrated in the z direction has $Q=2$, an isotropic distribution has $Q=0$, and a distribution concentrated in the ρ direction has $Q=-1$. The evolution of Q for the full and half shells is shown in Fig. 14. In the half-shell case, the shell becomes much more peaked in the z direction, while in the full-shell case it stays fairly isotropic. This is because an oscillation can be set up against the increased depth of the potential. In the full-shell case, the shallow potential means that all pseudoparticles that experience significant interaction with the field are ionized by it; the particles that remain bound have their motion only slightly per-

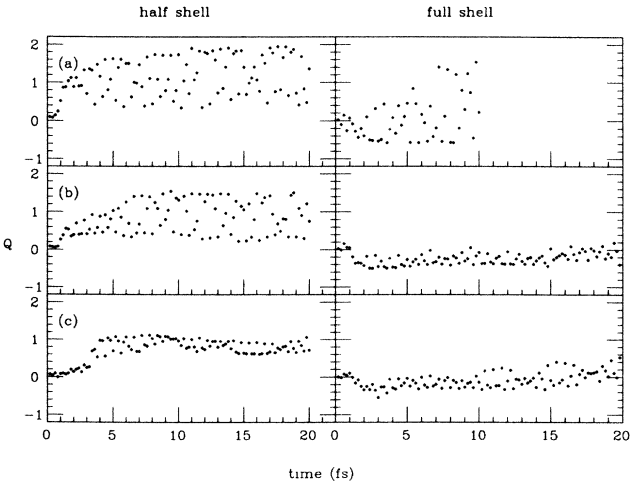

FIG. 14. Dimensionless quadrupole moments of the bound pseudoparticles as a function of time for both the initially full (right) and half-full (left) shells for $E_0=$ (a) 10.0, (b) 6.0, and (c) 3.0 V/Å.

turbed by the applied field. In the half-shell case, the potential is deeper and severely perturbed orbits can remain bound which allows a strong oscillation in the z direction to be built up. Thus, the magnitude of the driven oscillation is very sensitive to the potential and the starting distribution. However, the overall expansion of the shell, as shown by the increase of the rms radius with time is not.

In conclusion, the electron energy spectra and overall expansion of the bound shell with time appear to be independent of the details of the starting distribution. On the other hand, the details of the time evolution of the shell vary strongly with the initial configuration.

C. Effects of the ponderomotive potential and pulse shape

In the above sections we have considered the atomic response to a laser pulse whose amplitude is independent of time and position. In reality, the laser pulse has spatial and temporal dependence:

$$\mathbf{E}(\mathbf{x},t)=\mathbf{E}_0(\mathbf{x},t)\hat{\mathbf{z}}\sin(\omega t)\ . \tag{16}$$

The time variation of the envelope of the pulse causes it to deviate from being monochromatic. If the variation is slow compared to the period of the pulse then one can approximate the pulse as being monochromatic at each point during the evolution and hence calculations which make this assumption can be used to study the evolution. The primary effect of this slow variation in current experiments is to make significant amounts of the ionization occur before the pulse has reached its peak value, thus making it difficult to expose an atom to the strong fields discussed in Secs. III B and IIIC. Rapid rise times are required to accomplish such a feat, which results in great deviations from monochromaticity. The effect of this must be understood.

The spatial variation of the pulse also has significant effects. One effect is that the field an atom feels depends on its location, so that when a pulse is applied to a volume of atoms, the results are the superposition of responses to a range of strengths. More importantly, the spectrum of electrons emitted by a single atom is affected by the spatial variation of the pulse, as we now discuss in some detail.

In current experiments, the time scale over which the pulse varies is long compared to the time it takes an ionized electron to escape from the spatial extent of the pulse, so one can regard the strength of the pulse as being time independent as the electron exits it. For frequencies large compared to the time scale of the electron's motion, the effect of the spatial variation is to introduce an effective potential known as the ponderomotive potential,

$$V_{\text{pond}}(\mathbf{x},t)=\frac{1}{4m}\frac{E_0^2(\mathbf{x},t)}{\omega^2}\ , \tag{17}$$

which corresponds to the average energy of oscillation of a particle in a monochromatic field of frequency ω and strength E_0. If one averages out the fast (frequency ω) fluctuations of the velocity of the particle to find a drift velocity $\langle \mathbf{v} \rangle$, then the quantity

$$\tfrac{1}{2}m\langle \mathbf{v} \rangle^2+V_{\text{pond}}(\mathbf{x},t) \tag{18}$$

is a constant of the motion.[14]

It follows that an electron ionized at a point $(\mathbf{x},t)$ will gain an energy $V_{\text{pond}}(\mathbf{x},t)$ in exiting the pulse if we interpret the kinetic energy of the electron within the pulse as being $\frac{1}{2}m\langle \mathbf{v} \rangle^2$ as opposed to $\frac{1}{2}m\langle \mathbf{v}^2 \rangle$. By computing our energy spectra after slowly lowering the strength of our pulse to zero, our energy spectra should roughly correspond to the former case. Thus, we can approximate the effect of the ponderomotive force by adding in energy V_{pond} to each ionized pseudoparticle. We saw in Sec. III A that this gives good agreement with experimental data. Of course, to account for the effect of a spatially varying pulse in our simulations exactly, we need to insert explicitly a spatially varying electromagnetic field. This is complicated by the fact that the variation of $\langle \mathbf{v} \rangle$ is influenced as much by the magnetic field as the electric field, so simply putting a spatially varying electric field into our calculation would not give a correct description of ponderomotive force. For discussions of the ponderomotive force within the context of quantum mechanics see Ref. 15.

For pulses that vary quickly in either time or space, the above analysis no longer holds. For instance, if the pulse envelope varies slowly in time compared to the period of the wave then no energy will be transferred to a free electron. If, instead, the pulse envelope varies quickly in time then one can transfer energy of order the ponderomotive energy to the electron. Similarly, if the pulse envelope varies rapidly in space then the energy transfer to the electron cannot be described via a simple potential.[16]

We now analyze the effect of short pulse lengths on the ionization of the full xenon shell. Using Gaussian envelopes

$$E_0(t)=E_0\exp\left[-\frac{(t-t_{\max})^2}{\sigma^2}\right]\sin(\omega t+\phi)\ , \tag{19}$$

we present results for $\omega=10^{16}$ sec^{-1} and $E_0=10$ V/Å with σ and ϕ varying. We start integrating the equations of motion at $t=0$ with $t_{\max}=3\sigma$.

In Fig. 15 we show the fraction of pseudoparticles ionized as a function of σ for $\phi=0$ and $\pi/2$. The amount of ionization levels off at around 1 fs corresponding to about

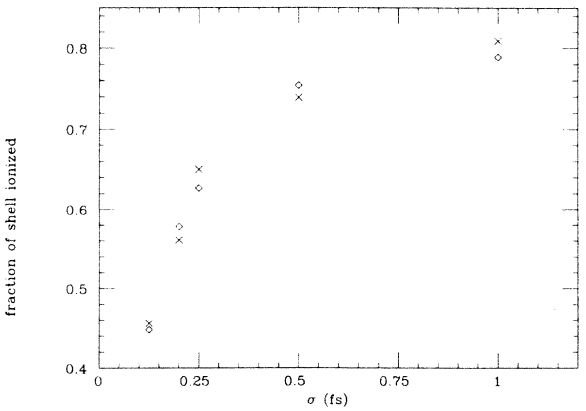

FIG. 15. Fraction of ionized pseudoparticles as a function of pulse width for phases $\phi=0$ (diamonds) and $\phi=\pi/2$ (crosses).

four periods of the pulse. We see from Fig. 1 that this is less than the ionization created by a monochromatic field of the same peak strength, which is expected since most of the ionization occurs when the pulse is less than its peak value. The results are reasonably insensitive to the phase of the pulse. Figure 16 shows the total ionization as a function of time superimposed on the pulse envelope. We see that as the pulse length becomes larger, ionization occurs earlier with respect to the peak. By the time $\sigma = 1$ fs all of the ionization has occurred before the pulse reaches its peak.

We now examine the energy spectra of the ionized pseudoparticles. In Fig. 17 we show the average energy as a function of E_0 for the two different phases. For short pulses, the average energy is very sensitive to the phase. The average energy peaks at about 0.25 fs and then decreases with increasing pulse width. This is understood because as the pulse length increases, the ionization is occurring earlier in the pulse and therefore at lower field strengths, which implies less electron energy. On the other hand, at small widths, the pulse is not on long enough and hence does not have the time to transfer as much energy as a longer pulse. Figure 18 shows the actual electron energy spectra. Comparing the spectra of the long pulses with that of the monochromatic waves, we see that the pulses have caused the spectrum to have a larger region of uniformity before the decaying tail sets in. This is presumably an effect of the ionization occurring for a range of strengths. As the pulses become shorter one sees significant dependence of the shape of the spectra on both pulse length and phase.

We also observe that the state of the remaining bound part of the atom varies strongly with the pulse width. Figure 19 shows the average energy of a bound pseudoparticle as a function of pulse length and phase. The results are insensitive to the phase. We see that there is a minimum over 0.25 fs.

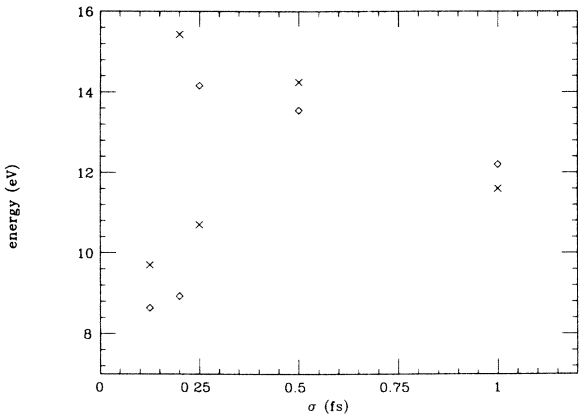

FIG. 17. Average energy of ionized pseudoparticles as a function of pulse width. The diamonds correspond to $\phi = 0$ and the crosses to $\phi = \pi/2$.

IV. CONCLUSIONS

We have investigated the evolution of an atomic shell in a strong, external field using a collective, semiclassical model and considering both monochromatic waves and short pulses. For the case of the monochromatic applied field, although many of the specifics of the evolution of the atom with time are sensitive to the initial conditions chosen for the shell, several features appear to be independent of the initial conditions. One of these is the expansion of the coherently driven shell with time. This occurs because as the shell ionizes, the potential in which the shell exists extends further in space. The external field pumps energy into the shell, causing it to expand out into the potential. Another is the envelope of the spectra of the ionized electrons. The shape and scaling of the

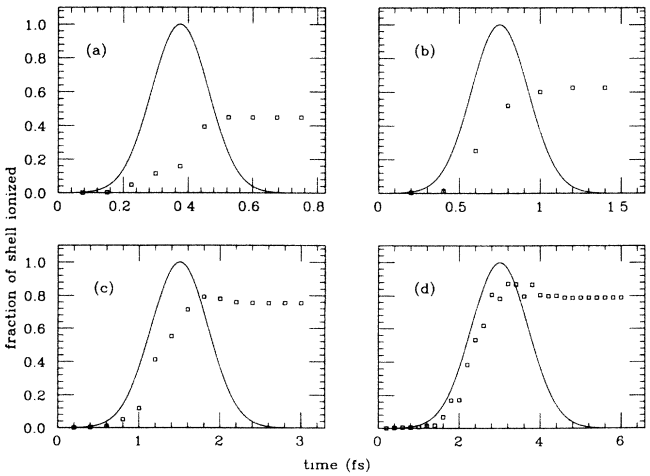

FIG. 16. Fraction of ionized pseudoparticles as a function of time for $\sigma =$ (a) 0.125, (b) 0.25, (c) 0.5, and (d) 1.0 fs. The solid line represents the shape of the applied pulse.

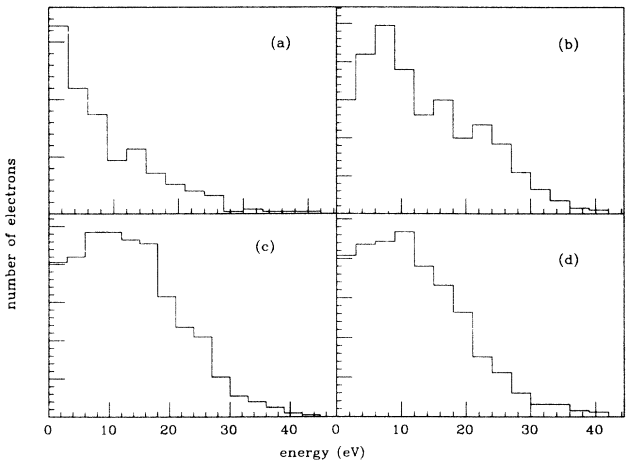

FIG. 18. Energy spectra of the ionized pseudoparticles for $\sigma =$ (a) 0.125, (b) 0.25, (c) 0.50, and (d) 1.0 fs with $\phi = 0$.

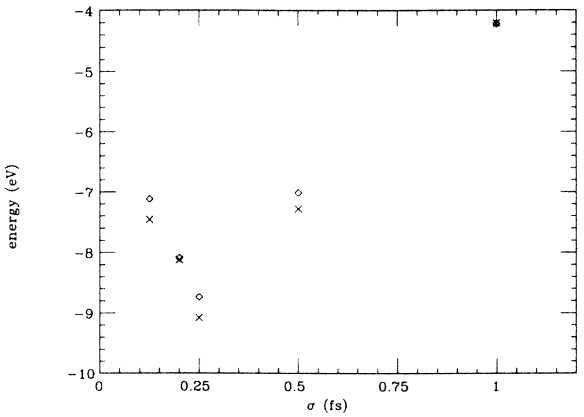

FIG. 19. Average energy of bound pseudoparticles as a function of pulse width. The crosses correspond to $\phi=\pi/2$ and the diamonds to $\phi=0$.

electron spectra, generated from collective ionization, also behave similar to the envelope of experimental spectra generated from single-electron ionization.

We have also examined the effect of pulsed waves on the atoms. As the rise time becomes of order the period of the wave, the response becomes very sensitive to the pulse length and phase, especially the ionized energy spectra. Finally, for longer pulse lengths, we have observed the ionization occurring earlier along the pulse. This is manifested in the declining average energy of the ionized electrons with pulse length.

Future calculations with this model could be improved by generating the initial electron distribution from the Wigner transformation rather than the Thomas-Fermi distribution. This would allow us to examine the effect of separation energy on the evolution of a neutral atom. Such calculations would be the best calculations possible with this model, and would allow direct comparisons with experimental data and with TDHF calculations.

ACKNOWLEDGMENTS

We acknowledge an allocation of time on the San Diego Supercomputer Center Cray X/MP-48, on which most of these calculations were performed. D.A.W. acknowledges financial support from AT&T Bell Laboratories. This work was also supported by National Science Foundation Grant Nos. PHY-85-05682 and PHY-86-04197.

[1]K. Boyer and C. K. Rhodes, Phys. Rev. Lett. **54**, 1490 (1985); A. Szöke and C. K. Rhodes, *ibid.* **56**, 720 (1986); M. Lewenstein, J. Phys. B **19**, L309 (1986); Z. Bialynicka-Birula and I. Bialynicka-Birula, Phys. Rev. A **33**, 1671 (1986).

[2]U. Johann, T. S. Luk, H. Egger, and C. K. Rhodes, Phys. Rev. A **34**, 1084 (1986).

[3]P. Lambropoulos, Phys. Rev. Lett. **55**, 2141 (1985).

[4]P. Kruit, J. Kimman, H. G. Muller, and M. van der Wiel, Phys. Rev. A **28**, 248 (1983); F. Yergeau, G. Petite, and P. Agostini, J. Phys. B **19**, L663 (1986).

[5]L-A. Lompré, G. Mainfray, C. Manus, and J. Kupersztych, J. Phys. B **20**, 1009 (1987).

[6]Y. Gontier and M. Trahin, J. Phys. B **13**, 4383 (1980).

[7]A. L'Huiller, L. Jönsson, and G. Wendin, Phys. Rev. A **33**, 3938 (1986).

[8]K. C. Kulander, Phys. Rev. A **35**, 445 (1987); **36**, 2726 (1987).

[9]T. S. Luk, U. Johann, H. Pummer, and C. K. Rhodes, Phys. Rev. A **32**, 215 (1985).

[10]C.-Y. Wong, Phys. Rev. C **25**, 1460 (1982); J. Aichelin and G. Beutsch, *ibid.* **31**, 1730 (1985).

[11]E. Uehling and G. Uhlenbeck, Phys. Rev. **43**, 552 (1933).

[12]C. L. Kirschbaum and L. Wilets, Phys. Rev. A **21**, 834 (1980); W. A. Beck, Jr., Masters thesis, University of Washington, 1984 (unpublished).

[13]D. A. Wasson (unpublished).

[14]See, e.g., G. W. Kentwell and D. A. Jones, Phys. Rep. **145**, 319 (1987).

[15]A. Szöke, J. Phys. B **18**, L427 (1985); L. Pan. L. Armstrong, Jr., and J. H. Eberly, J. Opt. Soc. Am. B **3**, 1319 (1986); W. Becker, R. R. Schicher, and M. O. Scully, J. Phys. B **19**, L785 (1986).

[16]D. A. Wasson (unpublished).